

Far-Field Radiative Thermal Rectification Based on Asymmetric Emissivity

Ryan C. Ng,^{*} Alexandros El Sachat, Julianna Jaramillo-Fernandez, Clivia M. Sotomayor-Torres, and Emigdio Chavez-Angel^{*}Cite This: *ACS Appl. Opt. Mater.* 2024, 2, 973–979[Read Online](#)

ACCESS |

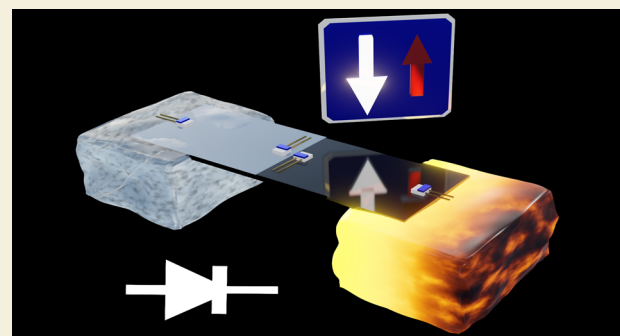
Metrics & More

Article Recommendations

Supporting Information

ABSTRACT: This experimental study investigates thermal rectification via asymmetric far-field thermal radiation on a fused silica slab. An asymmetrical distribution of surface emissivity is created over the device by partially covering the fused silica with a 100 nm thick aluminum film. The slab is subjected to a thermal bias, and when this bias is reversed, a small temperature difference is observed between the different configurations. This temperature difference arises from the difference in emissivity between the aluminum layer and fused silica, resulting in the transfer of thermal energy to the surrounding environment through radiation. Experimental findings are supported by finite element simulations, which not only confirm the measured values but also provide valuable insights into the rectification efficiency of the system. The rectification efficiency is found to be approximately 50% at room temperature for a thermal bias of 140 K. Simulations, which are performed by considering different environmental conditions experienced by the radiation and free convection processes, provide further insight into the underlying thermal rectification mechanism. These simulations consider an environmental temperature of 4 K for thermal radiation and an ambient temperature of 294 K for free convection and reveal an enhanced rectification effect with a rectification efficiency up to 600% when a thermal bias of 195 K is applied. This result emphasizes the significance of considering both convection and radiation in the thermal management and rectification of asymmetric systems. The outcomes of this study further our understanding of the thermal rectification phenomenon. They also show the importance of system asymmetry, emissivity disparities, environmental conditions, and the interplay between convection and radiation. Furthermore, the findings have implications for heat transfer and rectification in asymmetric systems, offering potential applications in areas such as energy harvesting, thermal management, and heat transfer optimization in electronic devices.

KEYWORDS: far field thermal radiation, thermal rectifier, radiative cooling, asymmetric thermal radiation, thermal management



transfer coefficient (h). This represents the rate of heat transfer per unit area between a surface and surrounding fluid per unit temperature difference between them. Careful engineering and optimization of the conduction, convection, and thermal radiation mechanisms can significantly enhance the heat transfer efficiency in various applications. In this context, thermal rectification is an especially intriguing phenomenon for thermal management.^{6–8}

Thermal rectification is a phenomenon in which heat flow through a material is directionally dependent such that the heat current is more efficient in one direction than its opposite

INTRODUCTION

The efficient operation of faster electronic devices and the trend toward miniaturization have intensified the need for effective thermal management techniques and the study of heat propagation.^{1–4} Heat transfer occurs through three primary mechanisms: conduction, convection, and thermal radiation.⁵ Conduction involves the transfer of heat through a solid material due to molecular interactions, where heat energy flows from regions of higher temperature to regions of lower temperature. Convection relies on the movement of a fluid (liquid or gas) to transport heat energy. Radiation involves the transfer of heat through electromagnetic waves without the need for a medium or direct contact between the heat source and the heat sink. This mechanism depends on the emissivity (ϵ) of the material, which characterizes its efficiency in emitting thermal radiation. The quantification of the efficiency of heat transfer between a solid surface and a moving fluid (liquid or gas) is described in terms of the convective heat

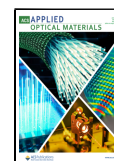
Special Issue: Optical Materials for Radiative Cooling

Received: July 7, 2023

Revised: August 30, 2023

Accepted: August 31, 2023

Published: September 29, 2023



direction. This effect is significant in nanoscale materials, where the mismatch between the phonon spectra of different materials at an interface results in asymmetric thermal transport. The ability to rectify heat flow is crucial for the development of advanced thermoelectric devices,^{9–11} thermal diodes,^{6,12} thermal transistors^{6,13–16} and thermal logic gates.^{16–18} Thermal rectification can be described as a nonlinear and asymmetric process where the thermal characteristics of a material along a specific axis depend on the direction of the temperature gradient or the heat current.¹⁹ In solid-state systems, various mechanisms have previously been proposed to achieve thermal rectification. These mechanisms include, but are not limited to, variations in thermal boundary resistances between two materials,^{20–23} the presence of anharmonic interatomic potentials,²⁴ dissimilar bulk materials exhibiting distinct temperature-dependent thermal conductivities (k),^{25–27} and the use of asymmetrically structured materials (such as those involving load mass,²⁸ ballistic scattering,²⁹ mass gradient^{17,30,31} and asymmetric thermal radiation^{32–34}). While various metrics and definitions for the thermal rectification efficiency (η) are found in the literature,⁷ here we define by η as the ratio between the heat fluxes:^{25,33}

$$\eta = \frac{F_{\max} - F_{\min}}{F_{\min}} \quad (1)$$

where F_{\max} (F_{\min}) is the absolute value of the maximum (minimum) thermal flux. This ratio can also be multiplied by a factor of 100 to express the efficiency in terms of percentages, offering a more intuitive representation.

Within this context, the radiative thermal rectification (RTR) effect has emerged as a promising way for achieving directional heat flow.³⁴ This concept harnesses the directional nature of radiative heat transfer to create thermal rectifiers capable of regulating the heat flow in a controlled manner. By selective modification of the optical emissivity or absorption properties of the device, asymmetric thermal radiation can be generated, leading to significant temperature differences when the device operates in one direction versus the other. RTR is achieved both in the near field (NF) and in the far field (FF). NF rectification exploits evanescent waves and strong coupling that occur at extremely short distances, while FF rectification relies on directional radiative properties and propagating waves at larger distances. In the case of NF-RTR, rectification efficiencies as high as 13 (or 1300%) have been theoretically predicted to be achieved with extremely small gaps between SiC-3C nanoparticles under a thermal bias of 500 K.³⁵ In other studies, even larger rectification efficiencies have been predicted based on NF-RTR, indicating the immense potential of this approach.³³ However, it should be noted that realizing such small gaps and large thermal biases, especially when nanoparticles are involved, requires considerable challenges to be overcome. When comparing NF RTR to FF RTR, the latter offers the significant advantage of simplicity and ease of fabrication, as it does not require the combination and alignment of objects separated by micrometric or nanometric gaps.^{34,36–38} FF RTR, also known as radiative cooling, is a passive cooling mechanism in which an object can effectively dissipate heat by emitting thermal radiation to the colder surroundings, typically the sky.^{39–42} In this case, this phenomenon exploits the difference in temperature between an object and the atmosphere, with heat generally being

released (i.e., high material absorption/emissivity) over the atmospheric window in the infrared where there is limited optical absorption of thermal radiation by atmospheric gases. The advent of novel materials and designs has revolutionized radiative cooling, enabling subambient cooling even under direct sunlight.^{40,43,44} Under a different context, exploiting this effect for achieving thermal rectification represents a promising addition to the toolbox of heat transfer control.

Previously, Lee et al. reported FF-RTR using a polyethylene terephthalate (PET)-based rectifier.³² Their device consisted of a $7.375 \times 0.442 \times 0.25 \text{ mm}^3$ PET substrate ($\epsilon = 0.9$), with half of its surface coated by a 200 nm thick niobium film ($\epsilon = 0.4$). The rectification efficiency was determined by combining experimental temperature measurements with finite element simulations. To prevent convective heat transfer, the measurements were conducted under vacuum conditions (10^{-4} Torr). The authors reported a rectification efficiency of $\eta = 0.13$ (13%) for a thermal bias of $\Delta T = 30 \text{ }^{\circ}\text{C}$. Additionally, they predicted a maximum $\eta = 0.9$ (90%) through the strategic manipulation of the emissivity and thermal conductivity of the rectifier components (substrate and top cover) and the environmental temperature, i.e., the temperature of the heat sink of the radiative part, under vacuum conditions.

In this work, we further their analysis, investigating the asymmetric far-field radiative thermal rectification mechanism to examine the rectification efficiency in a simple configuration involving a partially coated fused silica slab. Our approach is akin to that followed by Lee et al.,³² although the investigation is extended to include the influence of convective heat flux, a larger thermal bias, and sink temperature on the convective and radiative thermal transfer mechanisms. Although excluding convective heat transfer aids in providing an analysis that is focused only on the radiative component, in many practical applications, the inclusion of convective heat transfer is crucial as many scenarios involve nonvacuum conditions (e.g., terrestrial environments) and leads to more accurate modeling and understanding of heat transfer processes.

Incorporating thermal convection in FF-RTR is vital for many applications, as it plays a pivotal role in microelectronic cooling, industrial heat exchangers, and energy-efficient thermal management systems, ensuring accurate predictions and optimal performance in these applications. Remarkably, despite the ease of fabricating the structure presented in this work and its relative simplicity, it exhibits a robust radiative thermal rectification effect.

METHODS

The radiative thermal rectifier is made by depositing a 100 nm thick aluminum film onto a $75.5 \times 25.5 \times 1.1 \text{ mm}^3$ fused silica slide (SPI suppliers) (see Figure 1). To establish an asymmetric thermal radiation profile, the entirety of the bottom surface of the slab was coated, while only half of the top surface was coated. This configuration predominantly concentrates thermal radiation into a specified region of interest within the device. Temperature measurements were then performed by placing an array of four Pt resistance thermometers (TH100PT, Thorlabs) glued onto the sample with silver paint to ensure good thermal conductivity through the contacts. The temperature readings were recorded using four multimeters (34461A, Keysight Technologies) interfacing with a custom MATLAB code. For controlled heating, one side of the sample was exposed to a hot plate acting as the high temperature reservoir, and the temperature was manually set and regulated using an external Pt-1000 resistor acting as a PID controller for the hot plate. All measurements were done at ambient room conditions with a constant

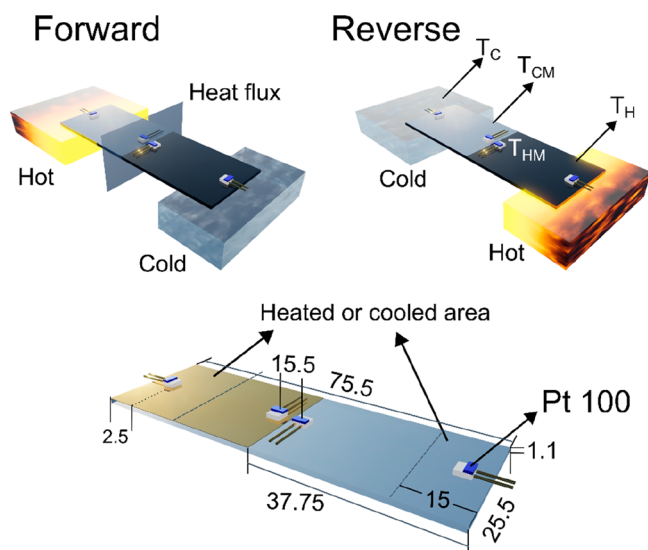


Figure 1. Schematic representation of the far-field radiative thermal rectifier. T_C , T_{CM} , T_H , and T_{HM} refer to the measured temperatures based on their proximity to either the cold or hot temperature reservoirs. T_C : directly above the cold reservoir. T_{CM} : close to the middle part of the rectifier and on the cold side of the slab. T_H : directly above the hot reservoir. T_{HM} : close to the middle part of the rectifier and on the hot side of the slab. The plane labeled with "heat flux" in the forward configuration represents the section of the slab where the heat flux was calculated. All dimensions are in mm.

environmental (lab) temperature of 294 K. The simulations to corroborate the experimental results in this work were performed with finite element method (FEM) performed with the commercially available COMSOL Multiphysics v.5.5 software. A detailed explanation of the simulations can be found in the [Supporting Information](#).

EXPERIMENTAL PROCEDURE

Thermal characterization was performed according to the following procedure:

1. The fused silica slab sample was positioned such that one side was placed on a hot plate, while the second side was in contact with a stainless-steel heat sink (forward configuration). This setup allowed for controlled heat transfer between the two halves of the slab. The ends of the slab were glued on top the reservoirs using silver paint to ensure good thermal contact.
2. The temperature of the hot plate was manually set to four different temperatures: 320, 340, 360, and 380 K. These specific temperatures were chosen to provide a range of thermal gradients for analysis.
3. Each temperature was maintained for a duration of 30 min to ensure that steady-state thermal equilibrium was achieved. This allowed sufficient time for heat to propagate and stabilize across the sample.
4. Following characterization in the forward configuration, the slab was also tested in the reverse configuration and was flipped to reverse the heat flow direction, and the experiment was repeated with the same temperature differences.

The temperatures were continuously recorded over the entire duration of the aforementioned experimental procedure. To facilitate data analysis, the measured temperatures were categorized based on their proximity to either the cold or hot temperature reservoir. Specifically, the temperatures recorded on the cold side were denoted as T_C (above cold reservoir) and T_{CM} (middle but on cold side), whereas the temperatures on the hot side were labeled as T_H (above hot reservoir) and T_{HM} (middle but on hot side). [Figure 1](#) schematically illustrates the two experimental forward and reverse configurations. In the forward configuration, the Al-coated part of the

slab was fixed onto the heated area, while in the reverse configuration, the Al-coated part was placed over the heat sink. This spatial arrangement introduced a fundamental asymmetry within the system, leading to the observed thermal rectification phenomenon. [Figure 2a](#)

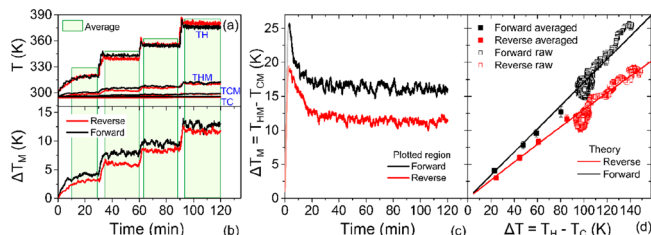


Figure 2. (a) Temperature distribution of the far-field radiative thermal rectifier for the forward (black) and reverse configurations (red line). (b) Temperature difference in the middle part of the rectifier $\Delta T_M = T_{HM} - T_{CM}$ as a function of time under the same conditions as in (a). (c) ΔT_M as a function of time for a thermal bias of $\Delta T = 100$ K. (d) Theoretical (lines) and experimental (squares) ΔT_M for forward (black) and reverse (red) configurations as a function of the thermal bias. The filled squares represent the average temperature shown in panels a and b, whereas the open squares represent the as measured temperature shown in panel c.

provides the temperature distribution over time for the radiative thermal rectifier, showing data for both the forward (black line) and reverse (red line) configurations. The green boxes indicate the areas over which the temperature was averaged and used to estimate the temperature difference in the middle part of the rectifier ($\Delta T_M = T_{HM} - T_{CM}$) and the thermal bias ($\Delta T = T_H - T_C$) for both configurations. [Figure 2b](#) shows the temperature difference in the middle part of the rectifier (ΔT_M) as a function of time for both configurations. The green boxes indicate the areas over which the temperature was averaged and used to estimate ΔT_M and ΔT for both configurations. [Figure 2c](#) presents a 2 h measurement of ΔT_M for a thermal bias of $\Delta T = 100$ K for forward (black lines) and reverse (red line) configurations, respectively. The large difference in the thermalization times between [Figure 2b](#) and c is a consequence of the experimental setup. In [Figure 2c](#), the hot plate initially starts at room temperature and undergoes a sudden increase to $T_H = 398$ K. By contrast, in the case of the measurement shown in [Figure 2b](#), the temperature changes of the hot plate were gradually implemented in small increments. [Figure 2d](#) shows the experimental (squares) and theoretical (solid lines) dependence of ΔT_M with respect to the ΔT for the forward (black) and reverse (red) configurations. The averaged regions shown in [Figure 2b](#) are presented in [Figure 2d](#) using filled squares, whereas the as measured temperatures shown in [Figure 2c](#) are plotted using empty squares.

The temperature difference between ΔT_M values in the forward and reverse configurations can be attributed to the inherent asymmetry of the system. More specifically, the emissivity of the aluminum is close to zero,⁴⁵ while the fused silica exhibits an emissivity of approximately 0.9.⁴⁶ These same values were also experimentally measured and confirmed in this study, as depicted in [Figure S3 of the Supporting Information](#). This difference in emissivity leads to a small temperature difference as a fraction of the thermal energy injected into the slab is transferred to the surrounding environment through thermal radiation. Consequently, this emissivity difference induces an asymmetry in the total heat flux passing through the slab for the forward and reverse configurations, analogous to the behavior of an electrical diode under an electrical bias. [Figure 3a](#) shows the theoretical asymmetric heat flux, resembling a diode-like curve, as a function of the temperature difference of the conductive thermal reservoir. In an ideal thermal diode, a near-zero heat flux would be observed for a negative temperature difference. [Figure 3b](#) shows the simulated rectification efficiency of the measured device using eq 1. The efficiency shows an almost linear increase with

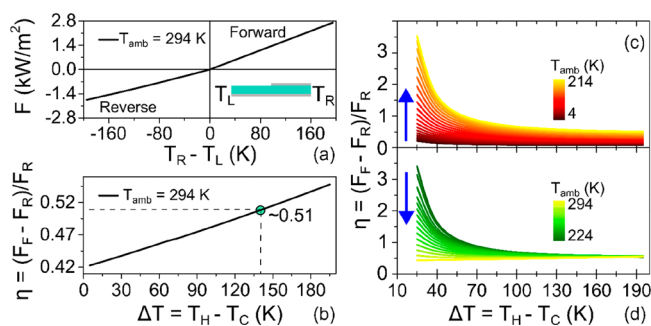


Figure 3. (a) Asymmetric heat flux (diode-like plot) as a function of the temperature difference of the conductive thermal reservoir ($T_R - T_L$) for $T_{\text{amb}} = 294$ K. Inset shows a representation of the T_R and T_L temperatures of the thermal reservoir fixed in the rectification slab. Rectification efficiency at varying ambient temperature: (b) at 294 K, (c) from 4 to 214 K, and (d) from 224 to 294 K.

increasing thermal bias ranging from 0.42 to 0.51 ($\Delta T = 5$ to 140 K), representing the experimental bias conditions.

Lee et al.³² recently reported $\eta = 0.13$ (13%) under a thermal bias of $\Delta T = 30$ °C. The observed thermal rectification was attributed to the asymmetric nonlinear thermal radiation arising from a slight difference in the emissivity values between niobium (~ 0.4) and PET (~ 0.9). In their case, they observed a small decrease in η from 0.14 to 0.12 as the power was increased from 340 to 920 μW (i.e., temperature difference $\Delta T = T_H$ versus T_C in our case). These observations were associated with the dependence of the thermal conductivity of PET with respect to temperature. The thermal conductivity of PET increases from 0.7 to 1.0 $\text{W K}^{-1} \text{m}^{-1}$ as the temperature increases from 298 to 333 K, representing a 43% increase in k . Conversely, in our case, the thermal conductivity of the fused silica showed a smaller dependence on temperature, increasing from 1.36 to 1.66 $\text{W K}^{-1} \text{m}^{-1}$ over the 300 to 500 K temperature range,⁴⁷ which corresponds to a 22% increase in k . This smaller variation led to a negligible impact on the rectification efficiency as shown in Figure S5 in the Supporting Information.

To further elucidate this dependence on ambient temperature, Figure 3c and d show the simulated rectification for varying ambient temperature. In the FEM simulations, the environmental temperature was considered to influence both convection and radiation equally. Consequently, the radiation and free convection processes were set to the same ambient temperature (T_{amb}) throughout the simulations. The rectification efficiency (eq 1) exhibits two distinct behaviors with respect to T_{amb} . At low ambient temperatures (i.e., $4 \text{ K} < T_{\text{amb}} < 214 \text{ K}$), the rectification efficiency increases as the ambient temperature rises. However, a transition takes place as the temperature T_{amb} exceeds 224 K, leading to a maximum in η , followed by a subsequent decrease with further increases in T_{amb} . Between the aforementioned regions, within the temperature range of 214–224 K, a gradual transition in rectification efficiency is observed, as shown in Figure S4 of the Supporting Information. As T_{amb} increases within this range, the rectification efficiency η decreases for a thermal bias $\Delta T < 45$ K. However, beyond this threshold, η increases as T_{amb} continues to rise. For $T_{\text{amb}} = 294$ K (i.e., the ambient environmental temperature in the experiment), a linear increase with respect to the thermal bias was found (see Figure 3b). This observed behavior is directly related to the temperature of the heat sink (T_C), which is in equilibrium with the surrounding environment and, thus, is at the ambient temperature. It is important to note that any environmental temperature lower than that of the heat sink used for thermal conduction will induce a cooling effect in the device, and the temperature in the middle part of the rectifier will be less than the temperature of either the hot or cold reservoir. In other words, a distinct scenario arises when the heat sink temperature (i.e., the cold reservoir) in the calculation of thermal radiation is modified. This scenario becomes particularly relevant when experiments are conducted outside of a controlled laboratory environment, as the ambient temperature experienced by free

convection differs from thermal radiation conditions. In such cases, heat dissipation occurs through the emission of thermal radiation toward the sky (T_{sky}), exhibiting a radiative cooling behavior.^{39–42}

We further explore this concept of radiative cooling in Figure 4, which shows the impact of the sky temperature (T_{sky}) on ΔT_M and on

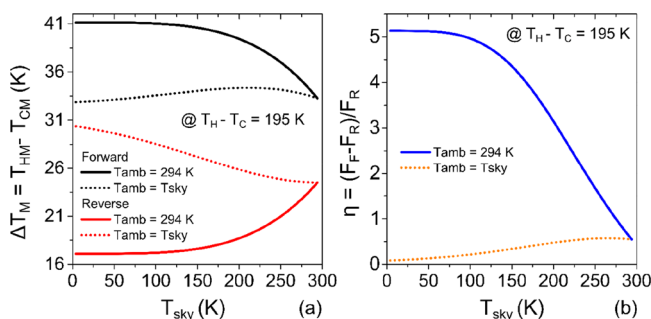


Figure 4. (a) Temperature difference in the central region of the rectifier (ΔT_M) as a function of the sky temperature (considered as the sink temperature for thermal radiation, T_{sky}) for a thermal bias of 195 K. The solid lines represent the simulated ΔT_M values when the ambient temperature is fixed at 294 K, while the dotted lines represent the simulated ΔT_M values when the ambient temperature is equal to the T_{sky} . (b) Thermal rectification efficiency was generated under the same conditions as described in panel a.

the rectification factor under a set thermal bias of $\Delta T = 195$ K. Two distinct scenarios were simulated: the first is the controlled temperature configuration in which $T_{\text{amb}} = T_{\text{sky}}$ and both free convection and radiation share the same thermal sink; the second is the radiative cooling configuration in which T_{amb} was fixed at 294 K for the free convection case, while T_{sky} varied for the thermal radiation case. In the radiative cooling configuration, a notable increase in ΔT_M between the forward and reverse configurations was observed (Figure 4a). The increased difference in ΔT_M leads to a larger rectification factor, as shown in Figure 4b. The results clearly indicate that the radiative cooling configuration enhances the rectification effect, resulting in a more significant thermal asymmetry in the system. Conversely, in the controlled temperature configuration, a smaller ΔT_M between the forward and reverse configurations was observed, which consequently leads to a smaller rectification factor. These differences can be easily understood by considering the boundary conditions of the problem. In the case of free convection, the environmental temperature affects the entire device uniformly and does not differentiate between the covered and uncovered parts of the rectifier, thereby impacting the overall device behavior. On the other hand, by fixing the environmental temperature for convection and varying only T_{sky} for thermal radiation, only the uncovered part of the rectifier is affected, inducing a larger temperature difference between the forward and reverse configurations. This, in turn, leads to a larger rectification factor, as depicted in Figure 4b.

The implications of both scenarios are significant for understanding the role of free convection and radiative cooling in thermal management. These findings underscore the importance of considering the specific boundary conditions and the interplay between free convection and radiative cooling in thermal systems. Understanding when to prioritize free convection versus radiative cooling enables us to design and optimize devices for specific applications, such as the case of thermal logic gates. By leveraging radiative cooling, we can enhance thermal rectification and create efficient thermal management systems, particularly in situations where generating significant thermal asymmetry is crucial as it is needed in the cooling of the electronics.

We also examine the influence of the absence of free convection, which is relevant for experiments conducted in controlled environments such as vacuum chambers or space applications. Figure 5a shows the impact of the absence of free convection (labeled as vacuum, blue dotted line) on the diode-like plot, with a comparison to

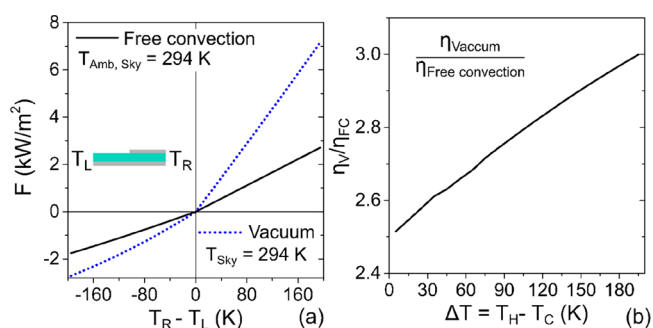


Figure 5. (a) Asymmetric heat flux (diode-like plot) as a function of the temperature difference of the conductive thermal reservoir ($T_R - T_L$) for a device subject to free convection (black solid line) and for a device in the absence of free convection (blue dotted line). (b) Ratio of the rectification efficiency for vacuum and free convection.

the sample subjected to free convection (black solid line). The results indicate a greater difference in the total heat flux, leading to a higher rectification efficiency in the absence of free convection. This difference stems from free convection acting as an additional cooling element for the entire rectifier, resulting in a reduced temperature distribution (see Figure S6a in the Supporting Information). The ratio of the rectification efficiencies (η) for both configurations is presented in Figure 5b. As the temperature increases, the difference between the rectification factors of the two configurations becomes more prominent. This effect is attributed to the larger temperature distribution difference, consequently leading to a greater heat flux induced by the radiative effect, in accordance with the Stefan–Boltzmann law.

Finally, the impact of omitting radiative thermal emission was also examined (see Figure S7 within the Supporting Information). By assigning an emissivity value of zero to the fused silica, we derived the temperature increase at the midpoint (ΔT_M) and the total flux through the slab center for both the forward and reverse configurations. The zero emissivity causes the thermal rectification effect to vanish with both the ΔT_M and total flux curves exhibiting the same patterns across both configurations. This result highlights that the emissivity and consequently the radiative transfer is key to the rectification effect that is observed here.

SUMMARY

This work investigated the thermal rectification phenomenon by exploiting asymmetric far-field thermal radiation. The introduced spatial arrangement, notably the presence of the deposited aluminum layer, played a crucial role in the observed thermal rectification effect, influencing the measured thermal distribution. The large difference in emissivity between the aluminum layer and fused silica resulted in a significant temperature difference, as a portion of the thermal energy was transferred to the surrounding environment through radiation. Experimental measurements, supported by FEM simulations, showed a significant difference in the temperature distribution between the forward and reverse configurations. In particular, the simulations revealed that the rectification efficiency exhibited different behaviors depending on ambient temperature. At low ambient temperatures (4–214 K), the rectification efficiency increased with respect to ambient temperature. However, a transition occurred at $T_{amb} > 224$ K, causing a decrease in the efficiency with further increases in T_{amb} . The exact temperatures at which these regimes occur depend specifically on the value of the ambient temperature in which the cold reservoir is in thermal equilibrium.

We looked more carefully at the special case of rectification, which may be outside of a controlled laboratory environment.

The different values of temperature for free convection and radiative transfer showed an amplified rectification phenomenon, resulting in a larger temperature difference (ΔT_M) between the forward and reverse configurations, and an augmented rectification factor. Conversely, the controlled temperature configuration exhibited a smaller ΔT_M and a diminished rectification factor, which is influenced by the uniform effect of the environmental temperature on the entire device. Furthermore, a significant enhancement of the rectification efficiency is observed in the absence of free convection, exceeding a factor of 2. This results from the temperature distribution and corresponding increase in heat flux through the slab, which can reach up to a factor of 3 with higher thermal biases. As the temperature distribution increases the radiative effect is enhanced in accordance with the Stefan–Boltzmann law.

These findings serve to improve our understanding of the radiative thermal rectification phenomena, providing valuable insights into system asymmetry, disparities in emissivity, environmental conditions, and the interplay between convection and radiation. The implications of these results extend to thermal management and rectification in asymmetrical systems, with more general widespread applications such as radiative cooling and other environmental applications, on-chip thermal logic gates or electronics under extreme thermal environments, or photonic metamaterials for temperature control, to name a few.

ASSOCIATED CONTENT

Supporting Information

The Supporting Information is available free of charge at <https://pubs.acs.org/doi/10.1021/acsaoam.3c00235>.

COMSOL simulations and the used parameters (Figure S1, Table S1 and Figure S2); Measurements of the optical properties of the slab (Figure S3); Smooth transition of rectification factor around 224–214 K (Figure S4); Impact of temperature dependence of the thermal conductivity (Figure S5); Impact of the absence of heat convection (Figure S6); Impact of the absence of emissivity (Figure S7); Photograph of device (Figure S8) (PDF)

AUTHOR INFORMATION

Corresponding Authors


Ryan C. Ng – Catalan Institute of Nanoscience and Nanotechnology (ICN2), 08193 Barcelona, Spain; orcid.org/0000-0002-0527-9130; Email: ryan.ng@icn2.cat

Emigdio Chavez-Angel – Catalan Institute of Nanoscience and Nanotechnology (ICN2), 08193 Barcelona, Spain; orcid.org/0000-0002-9783-0806; Email: emigdio.chavez@icn2.cat

Authors

Alexandros El Sachat – Institute of Nanoscience and Nanotechnology, National Center for Scientific Research “Demokritos”, 15341 Athens, Greece; orcid.org/0000-0003-3798-9724

Julianna Jaramillo-Fernandez – MIND-IN2UB, Departament d'Enginyeria Electrònica i Biomèdica, Facultat de Física, Universitat de Barcelona, 08028 Barcelona, Spain

Clivia M. Sotomayor-Torres – Catalan Institute of Nanoscience and Nanotechnology (ICN2), 08193 Barcelona, Spain; ICREA, 08010 Barcelona, Spain;  orcid.org/0000-0001-9986-2716

Complete contact information is available at: <https://pubs.acs.org/10.1021/acsaoam.3c00235>

Author Contributions

R.C.N.: validation, visualization, formal analysis, investigation, data curation and writing review and editing; A.E.S.: formal analysis and writing review and editing; J.J.F.: sample preparation, validation, writing review and editing; C.M.S.-T.: visualization, supervision, validation, project administration, and funding acquisition; E.C.-A.: conceptualization, visualization, formal analysis, investigation, methodology, software, validation, data curation, writing original draft preparation, and writing review and editing. All authors have read and agreed to the published version of the manuscript.

Notes

The authors declare no competing financial interest.

ACKNOWLEDGMENTS

ICN2 is supported by the Severo Ochoa program from the Spanish Research Agency (AEI, grant no. SEV-2017-0706) and by the CERCA Programme/Generalitat de Catalunya. R.C.N. acknowledges funding from the EU-H2020 Research and Innovation Programme under the Marie Skłodowska Curie Individual Fellowship (Grant No. 897148). A.E.S. acknowledges funding from the EU-H2020 research and innovation program under the Marie Skłodowska Curie Individual Fellowship THERMIC (Grant No. 101029727). C.M.S.T. acknowledges support by the AGAUR SGR-CAT grant Nr. 2021-0100.

REFERENCES

- Nadjahi, C.; Louahlia, H.; Lemasson, S. A Review of Thermal Management and Innovative Cooling Strategies for Data Center. *Sustain. Comput. Informatics Syst.* **2018**, *19*, 14–28.
- Cui, Y.; Li, M.; Hu, Y. Emerging Interface Materials for Electronics Thermal Management: Experiments, Modeling, and New Opportunities. *J. Mater. Chem. C* **2020**, *8* (31), 10568–10586.
- van Erp, R.; Soleimanzadeh, R.; Nela, L.; Kampitsis, G.; Matioli, E. Co-Designing Electronics with Microfluidics for More Sustainable Cooling. *Nature* **2020**, *585* (7824), 211–216.
- Feng, C.-P.; Chen, L.-B.; Tian, G.-L.; Wan, S.-S.; Bai, L.; Bao, R.-Y.; Liu, Z.-Y.; Yang, M.-B.; Yang, W. Multifunctional Thermal Management Materials with Excellent Heat Dissipation and Generation Capability for Future Electronics. *ACS Appl. Mater. Interfaces* **2019**, *11* (20), 18739–18745.
- Bejan, A. *Heat Transfer: Evolution, Design and Performance*, 1st ed.; John Wiley & Sons, Inc.: Hoboken, NJ, 2022.
- Wong, M. Y.; Tso, C. Y.; Ho, T. C.; Lee, H. H. A Review of State of the Art Thermal Diodes and Their Potential Applications. *Int. J. Heat Mass Transfer* **2021**, *164*, No. 120607.
- Malik, F. K.; Fobelets, K. A Review of Thermal Rectification in Solid-State Devices. *J. Semicond.* **2022**, *43* (10), No. 103101.
- Zhang, Y.; Lv, Q.; Wang, H.; Zhao, S.; Xiong, Q.; Lv, R.; Zhang, X. Simultaneous Electrical and Thermal Rectification in a Monolayer Lateral Heterojunction. *Science (80-)* **2022**, *378* (6616), 169–175.
- Benenti, G.; Casati, G.; Mejia-Monasterio, C.; Peyrard, M. From Thermal Rectifiers to Thermoelectric Devices. In *Thermal Transport in Low Dimensions. Lecture Notes in Physics*, Vol. 921; Lepri, S., Ed.; Springer: Cham, 2016; pp 365–407.
- Astrain, D.; Jaramillo-Fernandez, J.; Araiz, M.; Francone, A.; Catalán, L.; Jacobo-Martín, A.; Alegría, P.; Sotomayor-Torres, C. M. Enhanced Behaviour of a Passive Thermoelectric Generator with Phase Change Heat Exchangers and Radiative Cooling. *Appl. Therm. Eng.* **2023**, *225*, No. 120162.
- Hu, Z.; Mu, E. Application of Radiative Cooling in MEMS Thermoelectric Power Generation. *Infrared Radiative Cooling and Its Applications. Energy and Environment Research in China*; Springer: Singapore, 2022; pp 143–243.
- Liu, H.; Wang, H.; Zhang, X. A Brief Review on the Recent Experimental Advances in Thermal Rectification at the Nanoscale. *Appl. Sci.* **2019**, *9* (2), 344.
- Wang, L.; Li, B. Thermal Logic Gates: Computation with Phonons. *Phys. Rev. Lett.* **2007**, *99* (17), 177208.
- Hamed, A.; Ndao, S. NanoThermoMechanical AND and OR Logic Gates. *Sci. Rep.* **2020**, *10* (1), 2437.
- Ben-Abdallah, P.; Biehs, S.-A. Towards Boolean Operations with Thermal Photons. *Phys. Rev. B* **2016**, *94* (24), No. 241401.
- Hamed, A.; Elzouka, M.; Ndao, S. Thermal Calculator. *Int. J. Heat Mass Transfer* **2019**, *134*, 359–365.
- Ng, R. C.; Castro-Alvarez, A.; Sotomayor-Torres, C. M.; Chávez-Angel, E. Thermal Rectification and Thermal Logic Gates in Graded Alloy Semiconductors. *Energies* **2022**, *15* (13), 4685.
- Pal, S.; Puri, I. K. Thermal AND Gate Using a Monolayer Graphene Nanoribbon. *Small* **2015**, *11*, 2910.
- Roberts, N. A.; Walker, D. G. A Review of Thermal Rectification Observations and Models in Solid Materials. *Int. J. Therm. Sci.* **2011**, *50* (5), 648–662.
- Rogers, G. F. C. Heat Transfer at the Interface of Dissimilar Metals. *Int. J. Heat Mass Transfer* **1961**, *2* (1–2), 150–154.
- Powell, R. W.; Tye, R. P.; Jolliffe, B. W. Heat Transfer at the Interface of Dissimilar Materials: Evidence of Thermal-Comparator Experiments. *Int. J. Heat Mass Transfer* **1962**, *5* (10), 897–902.
- Clausing, A. M. Heat Transfer at the Interface of Dissimilar Metals—the Influence of Thermal Strain. *Int. J. Heat Mass Transfer* **1966**, *9* (8), 791–801.
- Zhao, J.; Wei, D.; Dong, Y.; Zhang, D.; Liu, D. Thermal Rectification Mechanism of Composite Cylinders with Temperature and Stress-Dependent Interface Thermal Resistance. *Int. J. Heat Mass Transfer* **2022**, *194*, No. 123024.
- Terraneo, M.; Peyrard, M.; Casati, G. Controlling the Energy Flow in Nonlinear Lattices: A Model for a Thermal Rectifier. *Phys. Rev. Lett.* **2002**, *88* (9), No. 094302.
- Dames, C. Solid-State Thermal Rectification With Existing Bulk Materials. *J. Heat Transfer* **2009**, *131* (6), 061301–061307.
- Kobayashi, W.; Teraoka, Y.; Terasaki, I. An Oxide Thermal Rectifier. *Appl. Phys. Lett.* **2009**, *95* (17), 171905.
- Go, D. B.; Sen, M. On the Condition for Thermal Rectification Using Bulk Materials. *J. Heat Transfer* **2010**, *132* (12), 124502–124504.
- Chang, C. W.; Okawa, D.; Majumdar, A.; Zettl, A. Solid-State Thermal Rectifier. *Science* **2006**, *314* (5802), 1121–1124.
- Lee, J.; Varshney, V.; Roy, A. K.; Ferguson, J. B.; Farmer, B. L. Thermal Rectification in Three-Dimensional Asymmetric Nanostructure. *Nano Lett.* **2012**, *12* (7), 3491–3496.
- Hahn, K. R.; Melis, C.; Colombo, L. Thermal Conduction and Rectification Phenomena in Nanoporous Silicon Membranes. *Phys. Chem. Chem. Phys.* **2022**, *24* (22), 13625–13632.
- Kasprzak, M.; Sledzinska, M.; Zaleski, K.; Iatsunskyi, I.; Alzina, F.; Volz, S.; Sotomayor Torres, C. M.; Graczykowski, B. High-Temperature Silicon Thermal Diode and Switch. *Nano Energy* **2020**, *78*, No. 105261.
- Lee, J.; Jan, A. A.; Ganorkar, S. P.; Cho, J.; Lee, D.; Baik, S. Tunable Solid-State Thermal Rectification by Asymmetric Nonlinear Radiation. *Mater. Horizons* **2021**, *8* (7), 1998–2005.
- Wen, S.; Liu, X.; Cheng, S.; Wang, Z.; Zhang, S.; Dang, C. Ultrahigh Thermal Rectification Based on Near-Field Thermal Radiation between Dissimilar Nanoparticles. *J. Quant. Spectrosc. Radiat. Transfer* **2019**, *234*, 1–9.

- (34) Sarkar, S.; Nefzaoui, E.; Basset, P.; Bourouina, T. Far-Field Radiative Thermal Rectification with Bulk Materials. *J. Quant. Spectrosc. Radiat. Transfer* **2021**, *266*, No. 107573.
- (35) Zhu, L.; Otey, C. R.; Fan, S. Ultrahigh-Contrast and Large-Bandwidth Thermal Rectification in near-Field Electromagnetic Thermal Transfer between Nanoparticles. *Phys. Rev. B* **2013**, *88* (18), No. 184301.
- (36) Chen, F.; Liu, X.; Tian, Y.; Zheng, Y. Dynamic Tuning of Near-Field Radiative Thermal Rectification. *Adv. Eng. Mater.* **2021**, *23* (2), 2000825.
- (37) Liu, X.; Wang, L.; Zhang, Z. M. Near-Field Thermal Radiation: Recent Progress and Outlook. *Nanoscale Microscale Thermophys. Eng.* **2015**, *19* (2), 98–126.
- (38) Fiorino, A.; Thompson, D.; Zhu, L.; Mittapally, R.; Biehs, S.-A.; Bezencenet, O.; El-Bondry, N.; Bansropun, S.; Ben-Abdallah, P.; Meyhofer, E.; Reddy, P. A Thermal Diode Based on Nanoscale Thermal Radiation. *ACS Nano* **2018**, *12* (6), 5774–5779.
- (39) Fan, S.; Li, W. Photonics and Thermodynamics Concepts in Radiative Cooling. *Nat. Photonics* **2022**, *16* (3), 182–190.
- (40) Jaramillo-Fernandez, J.; Whitworth, G. L.; Pariente, J. A.; Blanco, A.; Garcia, P. D.; Lopez, C.; Sotomayor-Torres, C. M. A Self-Assembled 2D Thermofunctional Material for Radiative Cooling. *Small* **2019**, *15* (52), 1905290.
- (41) Raman, A. P.; Anoma, M. A.; Zhu, L.; Rephaeli, E.; Fan, S. Passive Radiative Cooling below Ambient Air Temperature under Direct Sunlight. *Nature* **2014**, *515* (7528), 540–544.
- (42) Rephaeli, E.; Raman, A.; Fan, S. Ultrabroadband Photonic Structures To Achieve High-Performance Daytime Radiative Cooling. *Nano Lett.* **2013**, *13* (4), 1457–1461.
- (43) Zhao, B.; Hu, M.; Ao, X.; Chen, N.; Pei, G. Radiative Cooling: A Review of Fundamentals, Materials, Applications, and Prospects. *Appl. Energy* **2019**, *236*, 489–513.
- (44) Hossain, M. M.; Gu, M. Radiative Cooling: Principles, Progress, and Potentials. *Adv. Sci.* **2016**, *3* (7), 1500360.
- (45) *The Engineering Toolbox: Aluminum - Radiation Heat Emissivity*. https://www.engineeringtoolbox.com/radiation-heat-emissivity-aluminum-d_433.html (accessed June 27, 2023).
- (46) *The Engineering Toolbox: Surface Emissivity Coefficients*. https://www.engineeringtoolbox.com/emissivity-coefficients-d_447.html (accessed June 27, 2023).
- (47) Zeller, R. C.; Pohl, R. O. Thermal Conductivity and Specific Heat of Noncrystalline Solids. *Phys. Rev. B* **1971**, *4* (6), 2029–2041.